EO Africa // ARIES

D06 – Validation Methodology, Data and Results

Version 2.1, August 2024

Contract No: 4000139191/22/I-DT

submitted by

	VISTA Remote Sensing in Geosciences GmbH (VISTA) Vlaamse Instelling voor Technologisch Onderzoek, Naamloze vennootschap (VITO) Luxemburg Institute of Science and Technology (LIST)

ESA STUDY CONTRACT REPORT

ESA Contract No 4000139191/22/I-DT	SUBJECT EO Africa // ARIES		CONTRACTOR VISTA Remote Sensing in Geosciences GmbH (VISTA)
* ESA CR( )No	* STAR CODE	Vol. 1	* ESA CR( )No

ABSTRACT:

This document describes the validation methodology, validation data and validation results.

Version 2.1

Status: 28. August 2024

The work described in this report was done under ESA Contract. Responsibility for the contents resides in the author or organisation that prepared it.

Names of authors: Veronika Otto (Vista), Jeroen Degerickx (Vito), Louis Snyders (Vitoo), Silke Migdall (Vista), Kanishka Mallick (List), Aolin Jia (List)

** NAME OF ESA STUDY MANAGER Mr. Z. Szantoi DIV: EOP-SDR DIRECTORATE: Earth Observation Programmes	** ESA BUDGET HEADING

Authors of report

The present report was prepared by:

Veronika Otto, Silke Migdall

VISTA Geowissenschaftliche Fernerkundung GmbH

Gabelsbergerstr. 51, D-80333 Munich, Germany

Jeroen Degerickx, Louis Snyders

Vlaamse Instelling voor Technologisch Onderzoek, Naamloze vennootschap (VITO)

Kanishka Mallick, Aolin Jia

Luxemburg Institute of Science and Technology (LIST)

Content

Figures

Tables

List of Acronyms

ACF/AHH	Action contre la faim/Action Against Hunger
AGRHYMET	Centre régional de formation et d'application en agrométéorologie et hydrologie opérationnelle
AKTC	Zambian Agricultural Knowledge and Training Centre, LTD
CWC	Canopy Water Content
DMS	Data Mining Sharpener
ECOSTRESS	Ecosystem Spaceborne Thermal Radiometer Experiment on Space Station
EnMap	Environmental Mapping and Analysis Program
EO	Earth Observation
ESA	European Space Agency
ESI	Evaporative Stress Index
FAO	Food and Agriculture Organization of the United Nations
HR	High Resolution
ISMN	International Soil Moisture Network
KBDI	Keetch-Byram Drought Index
LAI	Leaf Area Index
LST	Land Surface Temperature
LWC	Leaf Water Content
MAE	Mean Absolute Error
ME	Mean Error
MODIS	Moderate Resolution Imaging Spectroradiometer
NASA	National Aeronautics and Space Administration
PRISMA	PRecursore IperSpettrale della Missione Applicativa
PWR	Plant Water Retrieval
R&D	Research & Development
RCMRD	Regional Centre for Mapping of Resources for Development
SAlib	Sensitivity Analysis Library
SDCI	hybrid Scaled Drought Condition Index
SM	Soil Moisture
SMAP	Soil Moisture Active Passive
STD	Standard Deviation
STR	Shortwave Infrared Transformed Reflectance
SWI	Soil Water Index
S3	Sentinel 3

1 Introduction

EO AFRICA (African Framework for Research Innovation, Communities and Applications) is a research and development initiative by ESA. It focuses on building African-European R&D partnerships and the facilitation of the sustainable adoption of Earth Observation and related space technology in Africa.

Within “ARIES” experimental EO analysis techniques are being developed and validated, addressing water management and food security in Africa.

To ensure the products developed within the project serve the needs of future users the techniques are being developed closely together with African Early Adopters. These five organizations are covering east (AfriGeo, EO research group within the Regional Centre for Mapping of Resources for Development in Kenya & the Regional Centre for Mapping of Resources for Development in Kenya itself), west (AGRHYMET Regional Centre and AAH Action Against Hunger in Niger) and southern (Zambian Agricultural Knowledge and Training Centre LTD in Zambia) Africa. Thereby the developed algorithms and approaches can be validated, tested and evaluated in different geographic regions with different climatic conditions and agricultural practices.

The current document aims to provide an overview of the validation methodology (Section 2), available validation data (Section 3) and validation results (Section 4) for all indicators developed within the framework of the ARIES project.

2 Validation Methodology

2.1 Direct Validation

Direct validation using field measurements will only be applicable to a few of our proposed products, for which measured data is available. For example, plant water content can be measured by the African partners by cutting a biomass sample and measuring the weight before and after drying to derive the difference between wet and dry biomass and thus the plant water content. Plant parameters that need more complex sensors to derive them in-situ like e.g., leaf area, are more difficult to procure, but can at least be compared to other leaf area products from multispectral satellite data.

2.2 Indirect Validation

Many of the proposed drought indicators cannot be directly measured on the field and are therefore hard to validate directly through field measurements. After careful interpretation of the computed drought indicators, parameters such as onset, duration and intensity of drought can be derived and qualitatively evaluated through observations made by the Early Adopters and/or existing drought monitoring platforms operating at low spatial resolution such as FAO's Agricultural Stress Index System. For this, already collected information on crop health/development, biomass production, yield, irrigation activities, and drought conditions will be made available for all reference sites of the Early adopters (Niger, Kenya, Mali, Senegal, Zambia; see Section 3.1 for full overview). By cross-checking temporal/spatial patterns in crop/pasture productivity with identified periods of ecosystem/crop water stress, we can obtain a good indication on the accuracy and usefulness of the developed indicators.

Although the final products might be hard to validate, there are some intermediate steps in the product generation workflows for which a more in-depth understanding of the accuracy can be gained. One example includes the evaluation of the Land Surface Temperature (LST) sharpening step, proposed to generate the high-resolution crop water stress indicators. Sharpened LST data derived from Sentinel-3 can be compared with high resolution LST data derived from both ECOSTRESS and Landsat 8/9 data. Although a direct comparison and strictly quantitative validation approach would be hard to obtain (due to differences in overpass time between the sensors), a more qualitative comparison of spatial and temporal patterns might already provide sufficient indication of sharpening accuracies.

2.3 Global sensitivity analysis

Aside from the (in)direct validation of the computed indicators and dedicated parts of the workflows used to generate the products, a global sensitivity analysis is planned to gain a better understanding of the primary driving factors behind the proposed indicators.

Global sensitivity/uncertainty analysis of the proposed drought indices due to uncertainty in input variables will be calculated using SOBOL-based uncertainty analysis (SAlib). Uncertainty analysis will be based on an assumed systematic error (caused by a potential bias in the input variables) at the study sites. In a first step, based on the literature, the error bounds of each input variable used for individual drought index estimation will be defined. The error samples (perturbation) within these bounds will be generated using the Saltelli sampling scheme (using the python package SALIB53) or in Matlab using appropriate packages. Each error sample will be added to the input variables. Actual input variables combined with perturbed input

variables will be used to estimate the drought indices. The obtained range in values of the individual drought index based on the perturbation will be used to calculate the uncertainty of our newly developed drought indicators.

2.4 Proposed Products and Envisaged Validation Methods

In Table 1 we provide an overview of the validation approaches which will be applied to each of the proposed indicators to be developed within ARIES.

Table 1 Proposed products and envisaged validation methods

Product	**Validation Method**	**Validation Data Description**
Green leaf area	Direct	LAI products from other satellites
Green leaf area	Indirect	In-situ measurements FLUX tower / biomass
Leaf / Plant water content	Direct	In-situ measurements of dry and wet biomass
Ecosystem water stress (70m)	Indirect	Comparison with biomass estimates derived from (1) field surveys and (2) low resolution satellite data analysis
High resolution crop water stress (10 – 20m)	Indirect	High resolution thermal satellite data to validate intermediate LST estimates. In-situ field-scale observations on biomass production, yield and crop water stress to validate the final crop water stress product.
Drought susceptible area	Indirect	In-situ field-scale observations on biomass production, yield and crop water stress
Canopy water content (30m)	Direct	In-situ measurements of dry and wet biomass
Canopy water content (30m)	Indirect	Intermediate steps in the product generation (green leaf area and leaf water content) can be validated through direct and indirect validation methods

3 Validation data

3.1 In-situ data

All associated Early Adopters either conduct or have access to agricultural tests sites (see Figure 1) in which they gather data relevant for validation of the planned innovative EO algorithms and products.

Figure 1 ARIES test sites in southern and western Africa

An overview of currently available in-situ reference data is presented in Table 2. The ground truth data was already collected in recent years and surveying continues so that validation data is available for the entire period covered by the project. This also ensures that in case no further data acquisitions of ECOSTRESS data can be conducted for the areas of interest during the project phase, historic data of recent years can be used to validate the EO algorithms and products.

Table 2 Available reference data sets for the African test sites

Organization	Country	Data available	Available variables	Years
ACF	Mali	Data on irrigated croplands	Crop type, crop damage, crop development anomaly and qualitative indication of crop yield	2023
	Senegal	Field campaigns conducted by CSE (Centre Suivi Ecologique), 61 active sites	Crop type; Crop health; Drought conditions; Pasture productivity	Since 1988, ongoing
AGRHYMET	Niger	Weather station data and field surveys, including multispectral UAV campaigns	Biomass availability in pastoral systems, soil moisture, temperature, wind speed, radiation	Ongoing for many years. Period of interest (2018 – 2022) is covered.
AKTC	Zambia	Weather station data, Data on drylands	Wet biomass, plant development (height, maturity, population, pests), Drought score, Soil type and chemistry	2022 - 2023
RCMRD	Kenya	Data collected at several sites throughout Kenya	Unknown but stated to support crop mapping and mapping of drought conditions	

With more validation data available for some of the test sites and less for others, incremental algorithm and product development and the initial validation will focus on certain test sites. The final products can then additionally be tested in one or several sites, that have not been used in development. This will provide a measure of transferability.

3.2 Other data sources

Low resolution satellite products, such as vegetation products from the Copernicus Global Land Service (e.g., dry matter productivity, LAI at 300 m resolution) and biomass/evapotranspiration products from FAO's WaPOR data portal (100 – 250 m) can also be used for validation in test sites with little or unsuitable in-situ data available, e.g., validation of green leaf area in pastoral test sites. Due to the products relatively coarse spatial resolution, especially in comparison with the products we are aiming to develop, their main use will be as an indicator for the temporal accuracy of our results. This will allow us to assess at least some aspects of the quality and usefulness of our products even in locations with little validation data available.

3.2.1 Soil Moisture

The International Soil Moisture Network (ISMN) is a collaborative initiative focussed on enhancing our understanding of soil moisture dynamics on a global scale. This network unites researchers, institutions, and organizations from around the world to collect, share, and analyze soil moisture data obtained from various sources and measurement techniques. By merging multiple networks, the ISMN facilitates comprehensive investigations into soil moisture variability across different spatial and temporal scales. Furthermore, the ISMN serves as a valuable resource for various stakeholders, including scientists, policymakers, and agricultural practitioners. By providing access to a wealth of soil moisture data and associated metadata, the network supports informed decision-making processes related to water resource management, agricultural planning, and climate adaptation strategies.

In Africa, the ISMN offers ground measurements from six networks, namely AMMA-CATCH, COSMOS, DAHRA, PBO_H2O, SD_DEM, and TAHMO. These networks collectively comprise 92 sites representing diverse climate and land cover types. Since ECOSTRESS data becomes available from July 2018, 36 sites has been utilized to illustrate the correlation between soil moisture and drought indices.

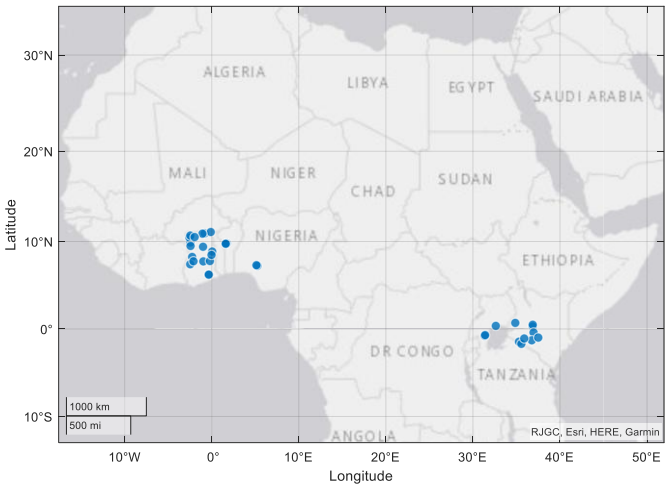

Figure 2 The ISMN soil moisture site distribution in Africa

4 Validation Results

4.1 Thermal Drought Indices

A correlation coefficient (cc) analysis was conducted across all ground sites to examine the relationship between ISMN SM and various drought indices. The corresponding statistical results are presented in Table 3. The median cc serves as a measure of overall performance, while the standard deviation (STD) is provided to account for variations in performance across different sites at 8-day and monthly scales.

Table 3 Median value at different sites and overall standard deviation (STD) statistics of Correlation coefficient (cc) between in-situ SM and drought indices.

Index	8-day		monthly	
	cc	STD	cc	STD
SMAP	0.85	0.07	0.88	0.11
SWI	0.88	0.12	0.91	0.21
KBDI	-0.47	0.17	-0.55	0.24
SDCI	0.40	0.15	0.44	0.24
STR	0.60	0.21	0.61	0.25
ESI	0.49	0.16	0.53	0.19

Table 3 reveals that SMAP and SWI exhibit the highest median correlation coefficients (cc) close to 0.9, with SMAP displaying significantly lower STD, signifying a more consistent performance across diverse conditions compared to ESA SWI. Notably, all meteorological and remote sensing drought indices fall short in capturing

the temporal variability of SM when compared to MW SM products. The cc values hover around 0.5, with a corresponding STD of 0.17. Notably, STR outperforms others, and post time upscaling, KBDI and STR demonstrate similar performance. ESI, with considerably fewer data points, exhibits a performance gap possibly attributed to data scarcity.

After removing the seasonality to detect the anomalous SM signals, the temporal variability of different drought index and soil moisture anomalies are shown in Figure 2.

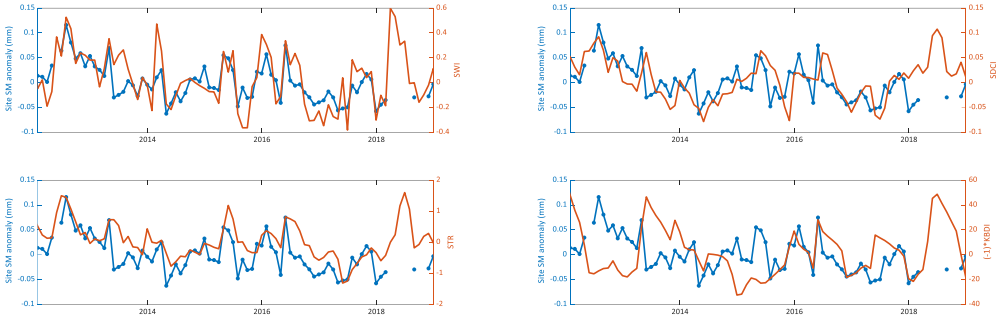

Figure 2 Drought indices captured the soil moisture anomalies (marked as blue)

In comparison, ECOSTRESS ESI shows the ability to map the drought stress at local scales. The Mali site (Lat: 16.6730 °, Long: -3.0448 °) was selected for local mapping analysis. The land cover type map (Figure 3) indicates the high heterogeneity around the site. The land cover type data is from Copernicus Global Land Cover Layers (CGLS-LC100) with 100m spatial resolution.

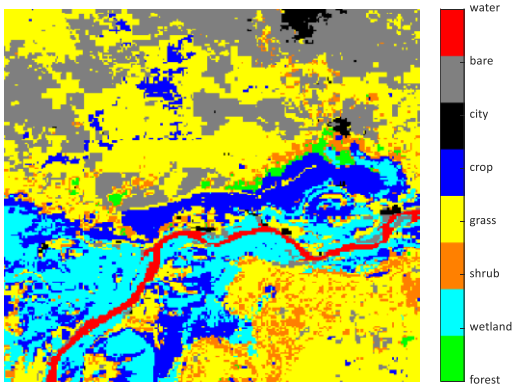

Figure 3 Land cover types surrounding the Mali site, and the spatial window size is 21 km.

The monthly ESI is subsequently mapped, revealing distinct temporal variations (Figure 4). Spatial patterns align closely with land cover characteristics, notably

indicating lower drought stress in wetlands during October in comparison to grassland and barren land (Fig. 4d). Figure 4 underscores the potential utility of ESI for localized drought stress monitoring.

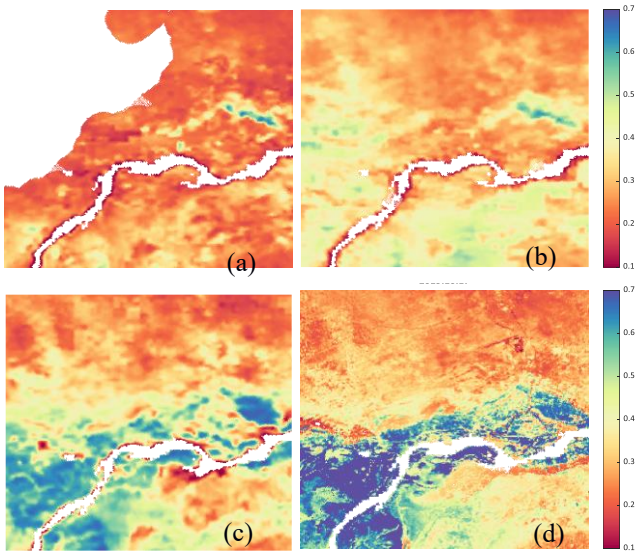

Figure 4 Monthly ESI maps at the Mali site (Lat: 16.6730 °, Long: -3.0448 °) in 2019 (a) July, (b) August, (c) September, and (d) October.

Even when averaging ESI images within a month, the ESI for July (Figure 4) exhibits a distinct data gap. This underscores the imperative to reconstruct the LST data, prior to its application to fully leverage drought indices derived from high-resolution remote sensing. The image comparison in Figure 5 with other indices demonstrates that high-resolution thermal data shows its better performance in mapping drought at local scales. In addition, due to the short span and limited sampling frequency of ECOSTRES data, detrending cannot be done, thus the seasonal cycle may also impact the results.

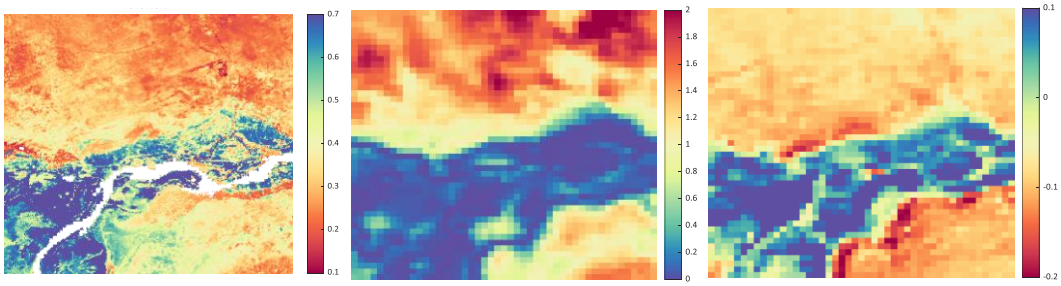

Figure 5 Local drought mapping using (a) ECOSTRESS ESI, (2) MODIS STR, and (3) MODIS NDWI

The overall recommendation of different drought indices is summarized in Table 4.

Table 4 Application recommendation of each drought index

	NASA SMAP soil moisture	ESA soil water index (SWI)	KBDI	MODIS STR	MODIS SDCI	ECOSTRESS ESI
Resolution	11 km	10 km	10 km	500 m	> 500 m	70 m
Data gaps	none	none	none	low	low	high
Forecasting	mid	low	high	low	mid	low
SM (dry) performance	great	great	great	good	bad	good
SM (wet) performance	great	good	bad	bad	bad	bad
SM anomaly	great	good	good	bad	good	-
Notes			drying season	arid	delay	
Input	microwave	microwave	Rainfall, air temperature	SWIR	NDVI, rainfall, LST	radiation, temperature, humidity …

4.2 Validation of high-resolution crop water stress indicator (20 m)

This section is divided into three parts. As this indicator is primarily based on a data sharpening procedure, converting low-resolution Sentinel-3 (S3) thermal data to a high-resolution land surface temperature (LST) product, the first section focusses on summarizing previous validation efforts related to thermal data sharpening. Within this project we have defined a procedure to improve the accuracy of the resulting sharpened LST product through direct comparison with high-resolution LST data from ECOSTRESS. The second section therefore focusses on highlighting the benefits of this two-stage correction procedure. Finally, in the third section, we focus on validation of the final crop water stress product based on in-situ reference data. First, the thermal sharpening validation section discusses the validation of the thermal sharpener, since it is the main input for our crop water stress indicator. The thermal sharpener is validated in literature, both theoretically and with in-situ data. Second, the cross-validation section, validates the thermal sharpened LST, the cross-calibrated LST and the directionally corrected LST by comparing S3 HR LST with ECOSTRESS LST.

4.2.1 Thermal sharpening validation

The thermal sharpener as used in this study has been previously validated in literature, both theoretically and with in-situ data. Guzinski & Nieto (2019) evaluated the feasibility of the proposed Sen-ET algorithm based on low-resolution thermal MODIS (1000 m) data and high-resolution VISNIR Landsat data. A comparison between high-resolution Landsat thermal data and MODIS sharpened thermal data showed similar spatial and temporal patterns, yet clearly lower LST contrast of the sharpened imagery compared to the high-resolution reference data.

Gao et al., (2012) used high-resolution Landsat LST as reference data and created low-resolution LST after aggregation of the reference data. The validation procedure sharpened the low-resolution LST with high-resolution reflectance bands and compared it with the reference data for three areas: a site with rainfed agriculture, a site with irrigated agriculture, and a site with natural vegetation and complex terrain. Table 5 shows the resulting mean absolute error for the three sites and different sharpening ratios. The utilization of the sharpening procedure adds additional uncertainty. The additional challenges include geo-referencing precision, different spectral bands than in the validation, differences in acquisition times, and variations in data quality. Important to note is that this particular validation study recommended a maximum sharpening ratio of 16, whereas sharpening S3 to S2 resolution corresponds to a sharpening ratio of 50.

Table 5 Mean absolute error (MAE) [K] of thermal sharpening methodology for three test sites and sharpening ratios from 2 to 16. The rainfed site shows the MAE range for three observations (Gao et al., 2012).

Sharpening ratio	Rainfed site	Irrigated site	Complex site
2	0.35-0.56	/	0.78
4	0.48-0.78	0.58	1.22
8	0.59-1.00	0.67	1.67
16	0.65-1.24	0.80	/

Sanchez et al. (2024) evaluated the performance of two sharpening methods, including the Data Mining Sharpener (DMS) used here, for the S3-S2 combination. The research reported an overall accuracy of 2.6 K for thermally sharpened LST from S2 and S3 data for croplands. Furthermore, the earlier observed reduced thermal range in thermally sharpened images was confirmed. More specifically, the LST of bare soil, which is typically high, is underestimated whereas the LST of vegetated areas, which is typically low, is overestimated. Additionally, the research observes an overall LST overestimation and explains this by pointing to the wrongly assigned land covers and

corresponding coefficients in the split-window algorithm of the Sentinel-3 LST retrieval algorithm.

4.2.2 Cross-calibration and directionality correction

As specified in the ATBD's, after thermal sharpening the high-resolution LST product derived from Sentinel-3 is going through a two-phase correction procedure to improve its overall quality: first, a cross-calibration with ECOSTRESS LST data takes place, followed by an explicit correction of directionality effects. This section validates the sharpened LST, the cross-calibrated LST and the directionally corrected LST through direct comparison with quasi-simultaneous high-resolution ECOSTRESS LST, as such showing the added value of the designed LST correction procedure.

- Methodology

  During cross-calibration, the available quasi-simultaneous Sentinel-3/ECOSTRESS observation pairs are split into two fractions: we use 80% of observations to train the cross-calibration and the directional model, and the remaining 20% of the observations to test the performance of the algorithm. Note that we use the 80%-20% for the observation pairs, not the number of pixels. To get stable results, 100 random training and test sets are generated from the observation pairs pool and validation is executed 100 times.

- Data

  This cross-validation exercise has been performed on Flanders, Belgium, for a period of three years covering 2019-2021. Flanders corresponds to three S2 tiles: 31UDS, 31UES and 31UFS. For this period 42 Sentinel-3/ECOSTRESS observation pairs were available. The region of Flanders has been selected due to ample availability of cloud-free Sentinel-3 and ECOSTRESS data.

- Results

  Figure 6 and 7 show the performance for each test-training set by showing the Mean Error (ME) and Mean Absolute Error (MAE), respectively. The ME shows a consistent LST overestimation for the original sharpened S3 data (S3 HR LST) and a consistent underestimation of the cross-calibrated version (S3 HR LST*). These results are in line with the expectations, since the split-window algorithm for the low-resolution S3 LST at 1000 meters overestimates temperatures, whereas S3 HR LST* still contains directional effects that generally decrease observed LST. This figure illustrates the strength of the methodology to remove

general bias in sharpened LST. The removal of this bias is of key importance for the development of the crop water stress indicator, which is not allowed to vary from day to day due to trends resulting from viewing geometry. While the Mean Error (ME) highlights the model's bias, the Mean Absolute Error (MAE) is equally crucial. Unlike ME, MAE reflects the overall error magnitude, irrespective of general bias. Thus, examining the MAE in Figure 6 and Figure 7 offers a more complete view of the model's performance and the methodology's effectiveness. The figure shows that the cross-calibration improves the original MAE from 2.11 K up to 1.80 K. After directional corrections, the MAE further improves to 1.62K. Overall, the proposed methodology decreases the MAE with 0.49 K, which is a 23% accuracy increase compared to the original sharpened LST product. Further improvements are expected by using a pixel-specific directional correction instead of the current generic correction.

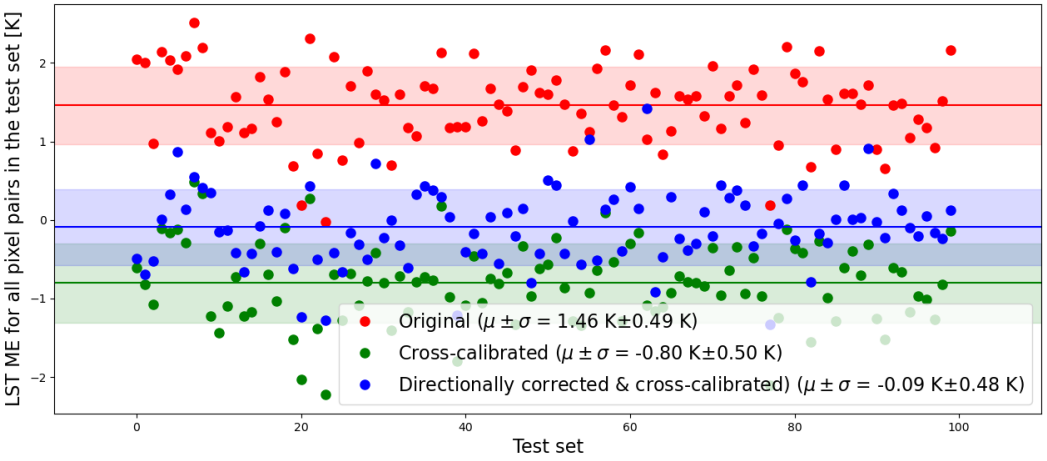

Figure 6 LST Mean Error (ME) of Sentinel-3 high-resolution LST compared to ECOSTRESS LST in a test set, for the original data (red), the cross-calibrated data (green) and the directionally corrected data (also cross-calibrated). The figure shows the results for 100 training-test sets based on all image pairs for Flanders from 2019-2022. Furthermore, the figure includes the mean and standard deviation of all test set MEs .

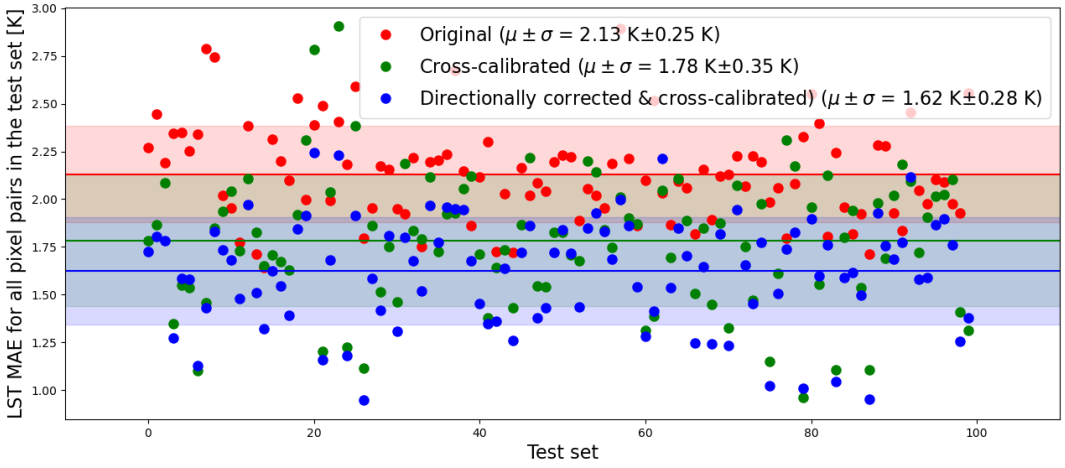

Figure 7 LST Mean Absolute Error (MAE) of the Sentinel-3 high-resolution LST compared to ECOSTRESS LST in a test set, for the original data, the cross-calibrated data and the directionally corrected data (also cross-calibrated). The figure shows the results for 100 training-test sets based on all image pairs for Flanders from 2019-2022. Furthermore, the figure includes the mean and standard deviation of all test set MAEs .

4.2.3 Validation of crop water stress indicator

The crop water stress indicator has been computed over the test sites located in Zambia (AKTC) and Mali (ACF). Some results for Zambia are summarized in Figure 8. Three important observations can be made based on this figure, confirming the LST-Ta indicator is working as intended and is indeed sensitive to crop water stress:

1) The LST-Ta indicator is highly sensitive to land cover, showing high values when the field is bare and low values when covered by a crop. This highlights the need to always account for land cover when interpreting this indicator (hence the inclusion of NDVI in the figure).

2) As can be seen in the left panel of the figure, LST-Ta indicator drops significantly following a major precipitation event, after which it slowly increases again. This is completely expected behaviour in a hot climate where water stress kicks in relatively quickly following a precipitation event.

3) During the growing season, the LST-Ta indicator shows distinctive peaks on the rainfed site, which are not present on the irrigated plot, indicating more crop water stress in the non-irrigated site, which is completely in line with expectations. This shows indeed that this specific indicator is sensitive to capturing the impact of irrigation practices on crop water stress, and potentially, productivity.

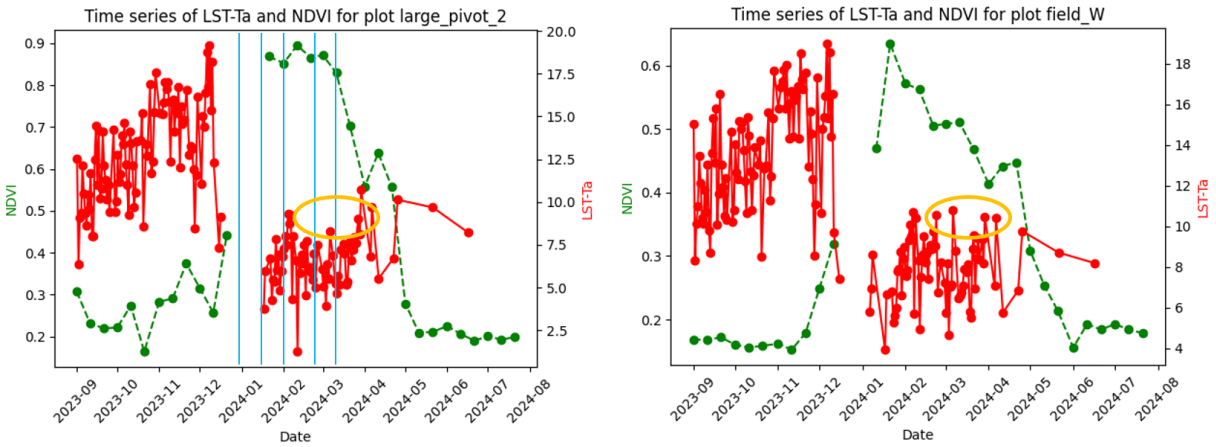

Figure 8 Crop water stress indicator (LST-Ta in red) and NDVI (in green) time series for two specific locations at the AKTC test site in Zambia during the main agricultural season in 2024: (left) a large pivot, representing irrigated agricultural fields, (right) a typical example of non-irrigated agricultural field. Blue lines represent major precipitation events, based on CHIRPS rainfall data extracted from the FAO WaPOR data portal. The orange circle in both figures highlight key difference in terms of crop water stress between the two sites.

When applying the crop water stress indicator to the Mali test sites, the limitations of the approach become apparent. As shown in Figure 9, left panel, for some fields the crop water stress indicator does make sense, showing relatively low values during the growing season, high values during periods of bare soil and a peak in crop water stress at the start of the growing season, matching the reported severity of drought for that particular field. On the other hand, the right panel of the same figure shows an example of a field where the derived crop water stress indicator shows no or limited correlation with land cover (as represented by the NDVI time series). This is a clear case where the results of the LST sharpening procedure cannot be trusted and final results should be interpreted with great care. This can be explained by considering the broader context of the specific agricultural field (Figure 10). Most of the area consists of desert, with only limited agricultural activities. In order for the LST sharpening approach to work, one needs a good amount of relatively homogeneous 1km x 1km pixels, especially over agricultural areas. On the Mali test site, this is clearly not the case, leading to unstable and unreliable high-resolution LST estimates. As said, this clearly implies the method cannot readily be applied anywhere. Future, higher spatial resolution thermal sensors will play a key role in alleviating this current limitation.

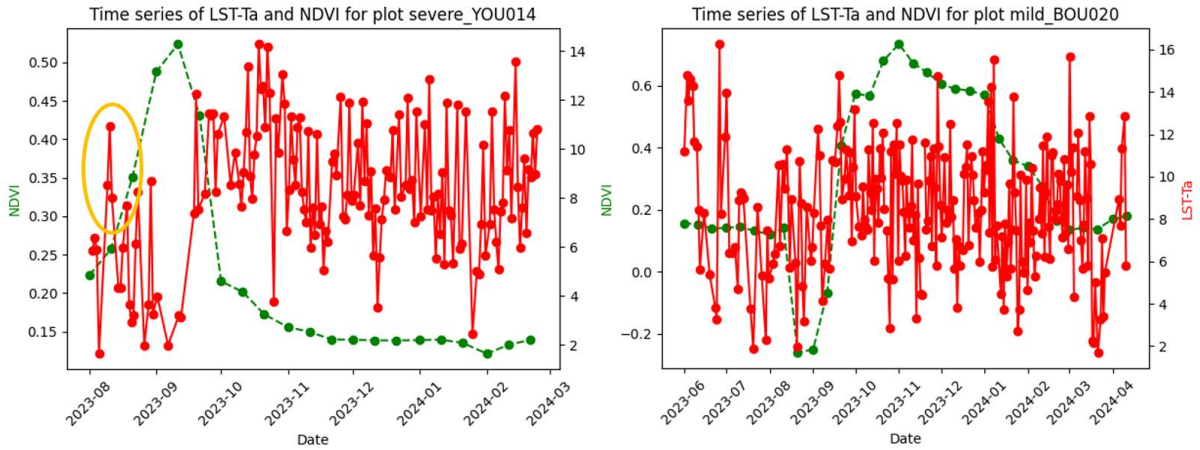

Figure 9 Crop water stress indicator (LST-Ta in red) and NDVI (in green) time series for two specific locations at the ACF test sites in Mali during the main agricultural season in 2024: (left) an agricultural field which is known to have faced severe drought at the start of the season and has been partially destroyed by wildlife, (right) an agricultural field that has faced only mild consequences from drought.

Figure 10 True color RGB image of the surrounding landscape for the Mali test site. The red dot identifies the specific field for which the LST-Ta and NDVI time series are shown in Figure 9, right panel.

4.3 Hyperspectral Product Validation

All initial product calculations (LAI, CWC, LWC) were done at the AKTC test site in Zambia, due the high number of EnMap and PRISMA data takes available (Figure 11 and Figure 12) and the good cooperation established with the site manager early on in the project. In the end, it was however not possible to acquire any quantitative in-situ data suitable for the validation of the calculated products. This was mainly due to timing issues and a mismatch in spatial resolution between the available in-situ data and the satellite data. The available in-situ data from small dryland plots (< 2 ha) was collected during the 2022/2023 rainy season, during which hyperspectral data acquisition for the test site was not yet established. Therefore, we opted for the use of external validation

data for the LAI product and sightly changed the calculation procedure of the plant water products. Instead of calculating the CWC from the inversely determined LWC and LAI, we used an established and calibrated method to calculate CWC (see D07_ATBD_PS_I), that has been validated before (Wocher et al. 2018).

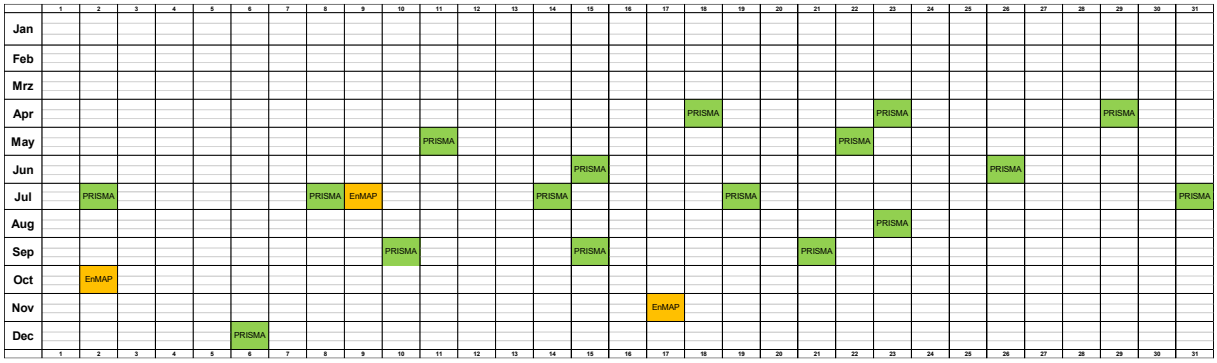

Figure 11 Available hyperspectral PRISMA and EnMap data takes at AKTC test site during 2023

Figure 12 Available hyperspectral PRISMA and EnMap data takes at AKTC test site as of August 2024

4.3.1 Validation of Leaf Area Index

LAI values were determined across the test site via model inversion of the PROSAIL model available within the EnMap toolbox. This was done for all available EnMap and PRISMA data takes (selected results in Figure 13) and a timeline of LAI results was created for several pixels within the irrigation pivots where wheat was being cultivated during the 2023 dry season (Figure 14). The area surrounding point 4 was not planted in 2023 (see Figure 13 Leaf Area Index results calculated from PRISMA data acquired during the 2023 dry season at AKTC Zambia.

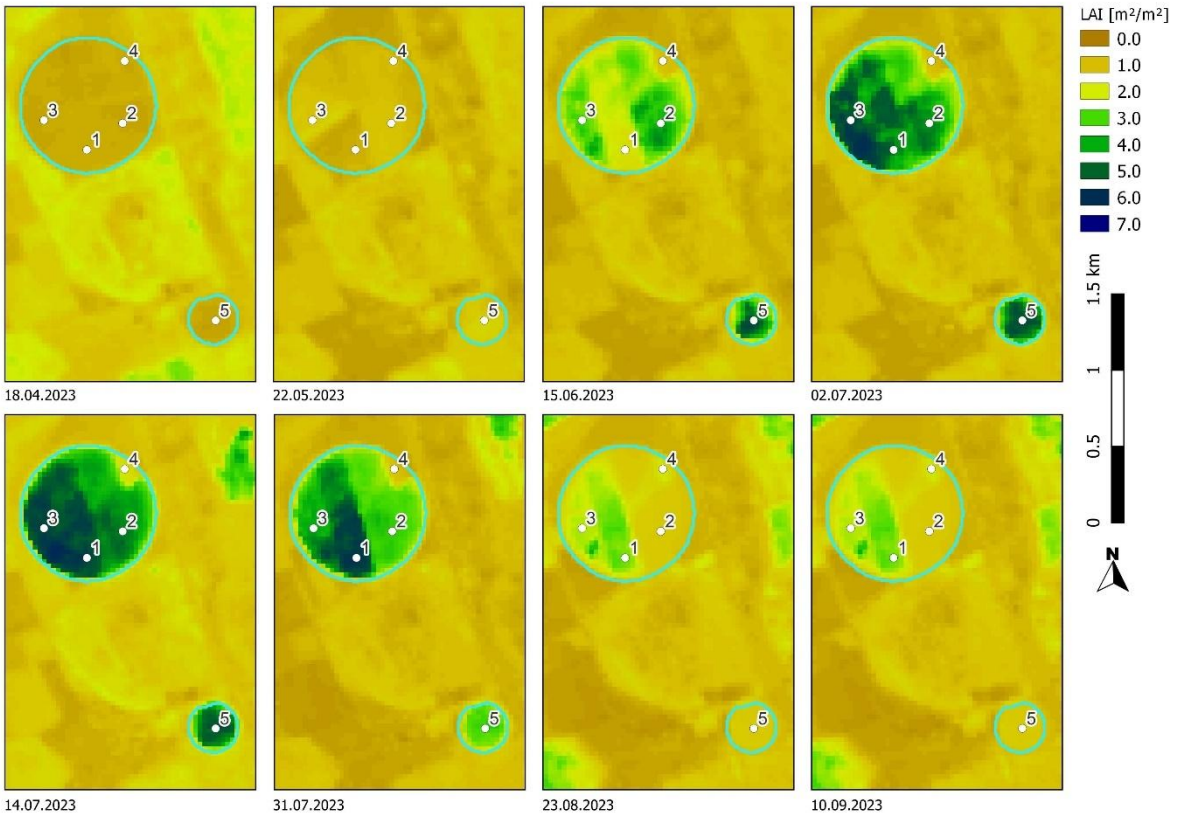

Figure 13 Leaf Area Index results calculated from PRISMA data acquired during the 2023 dry season at AKTC Zambia.

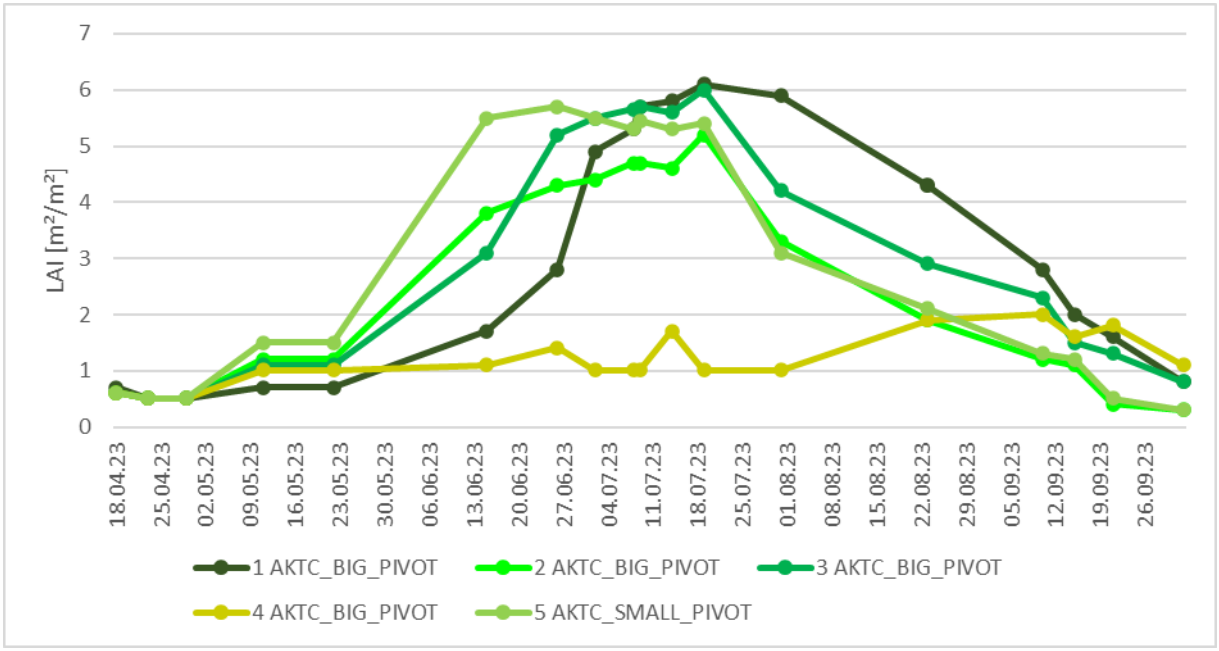

Figure 14 Leaf Area Index values calculated from PRISMA and EnMap data. Timeline at selected pixels within AKTC's irrigation pivots. Numbers correspond with locations indicated in Figure 13.

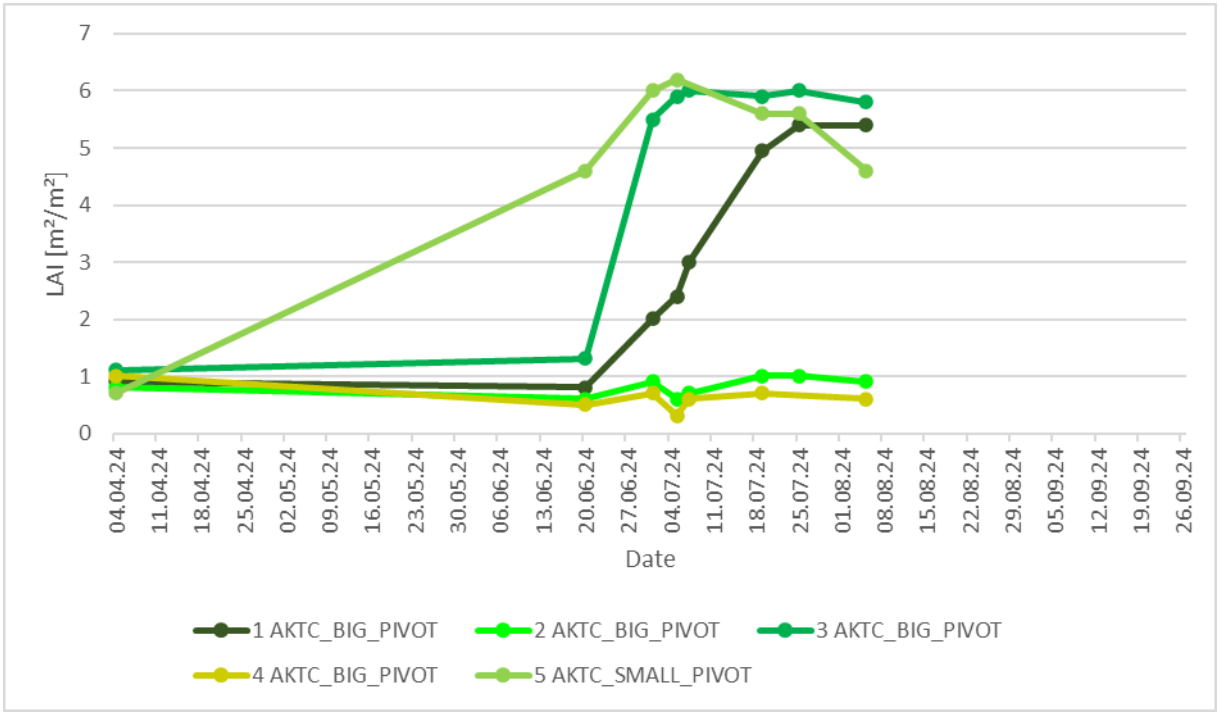

Figure 15 Leaf Area Index values calculated from PRISMA and EnMap data. Timeline at selected pixels within AKTC's irrigation pivots. Numbers correspond with locations indicated in Figure 13. The season is not over yet, hence LAI values stop in August. Between April and June there were no hyperspectral data takes.

As no quantitative leaf area or biomass in-situ data was available for the 2023 growing season, validation was based on mean LAI value results from both pivots, calculated from Sentinel-2 data from the last 3 years (2021 – 2023). Wheat has been grown on (parts of) the pivots in each of these years. LAI values were calculated for the pivots from Sentinel-2 multispectral data using a well-established method, which Vista has developed outside of this project and is using for its operational services, based on the SLC radiative transfer model (Verhoef & Bach 2007). LAI values were derived in a spatially distributed manner for all available high-quality Sentinel-2 data takes during the growing season for each of the years. Mean LAI values were calculated across all pixels inside the two irrigated pivots for each of the available dates. The values were then interpolated, so that one mean LAI value became available for each calendar day for comparison with the 2023 hyperspectral results (Figure 16).

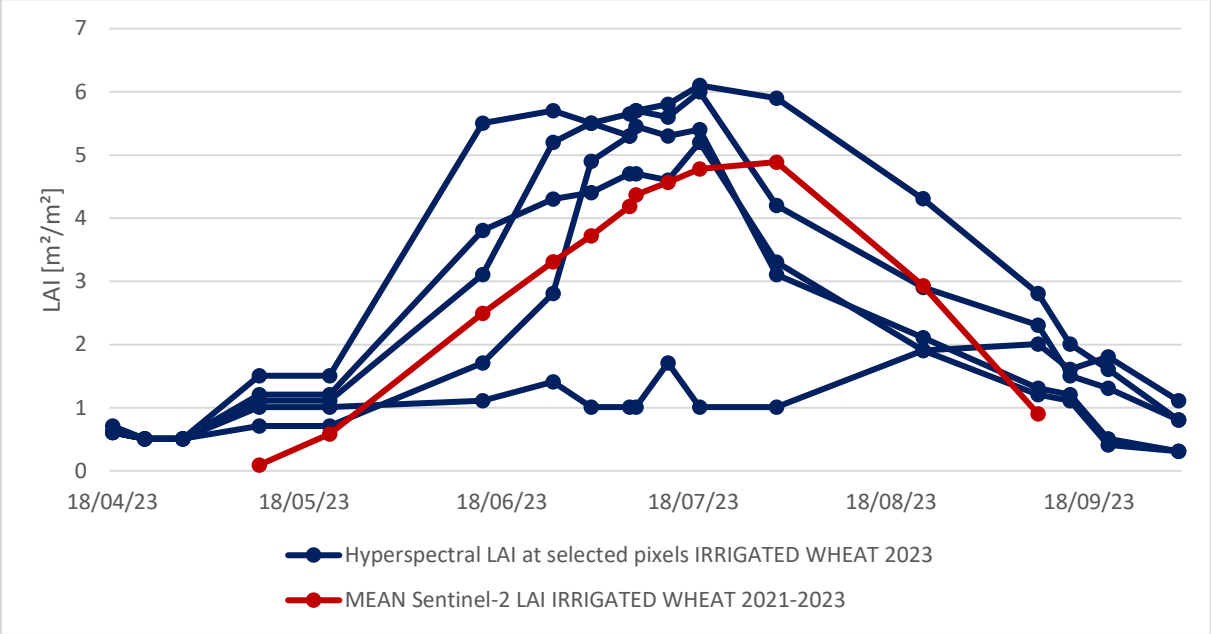

Figure 16 Comparison between mean LAI (2021-2023, across all pixels) calculated from Sentinel-2 data and LAI values from selected pixels calculated from hyperspectral data during the 2023 wheat growing season.

The Sentinel-2 based spatially distributed LAI product has been in use at AKTC for day-to-day farm management and informed decision making (e.g. with regards to irrigation amount and timing and determination of harvest time) for several years. The comparison (Figure 16) shows that while LAI is highly diverse across space - this variability is caused amongst other factors by planting dates, soil characteristics and management practice – the overall development of LAI throughout the growing season is similar between the mean Sentinel-2 LAI and the hyperspectral LAIs observed during the 2023 growing season.

An expert Interview with Mr Anschütz and Leslie De Jager from AKTC was conducted on 3rd June 2024. They could explain the differences in spatial development in the pivots seen in the LAIs in the 2023 time-series (Figure 13) as follows:

- At sample point 4 different varieties of potatoes were planted but didn't germinate
- Situation at end of May:
    - small pivot (point 5) was uniformly panted but there are differences in cultivation on the pivot
    - big pivot: not uniformly planted, differences in cultivation

- Differences might be caused by differences in cultivation in previous year. In winter: soy (cover crop)

- situation in June:
  - at sampling point 1: different variety, shorter but higher population
  - at sampling point 4: potatoes didn't germinate
  - sampling point 2 can be explained by germination differences

In general, there are some soil differences and germination differences of at least 10 days caused by disruptions in the farming practice (e.g. break downs). Planting dates also vary from year. This also needs to be acknowledged when comparing results from different years, so the heterogeneities seen in the 2024 data are also expected.

While no validation as such is planned in the Mali test-site for the hyperspectral products, the time-series was also calculated there and is shown in the following figures. Difference in LAI development are visible also in this drier area. Overall, the LAI values are smaller than in the irrigated fields in Zambia.

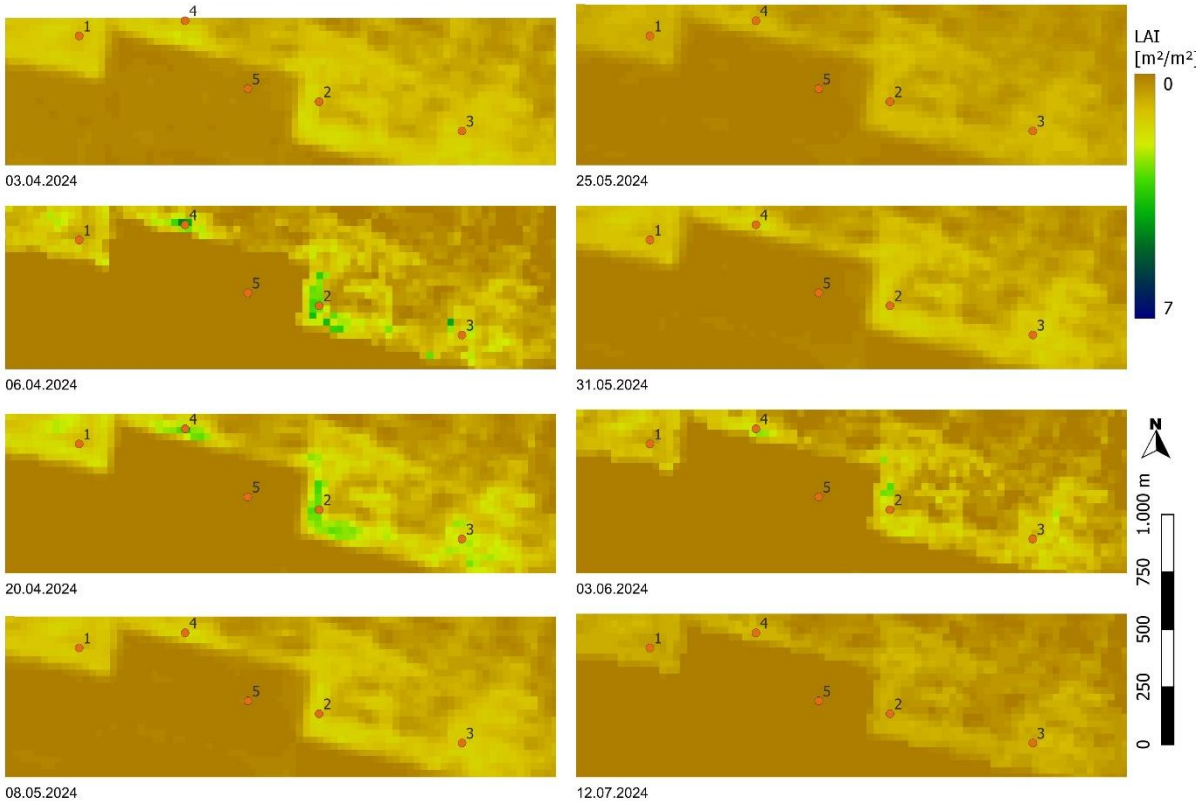

Figure 17 Leaf Area Index results calculated from PRISMA and EnMap data acquired during 2024 at the Mali test-site

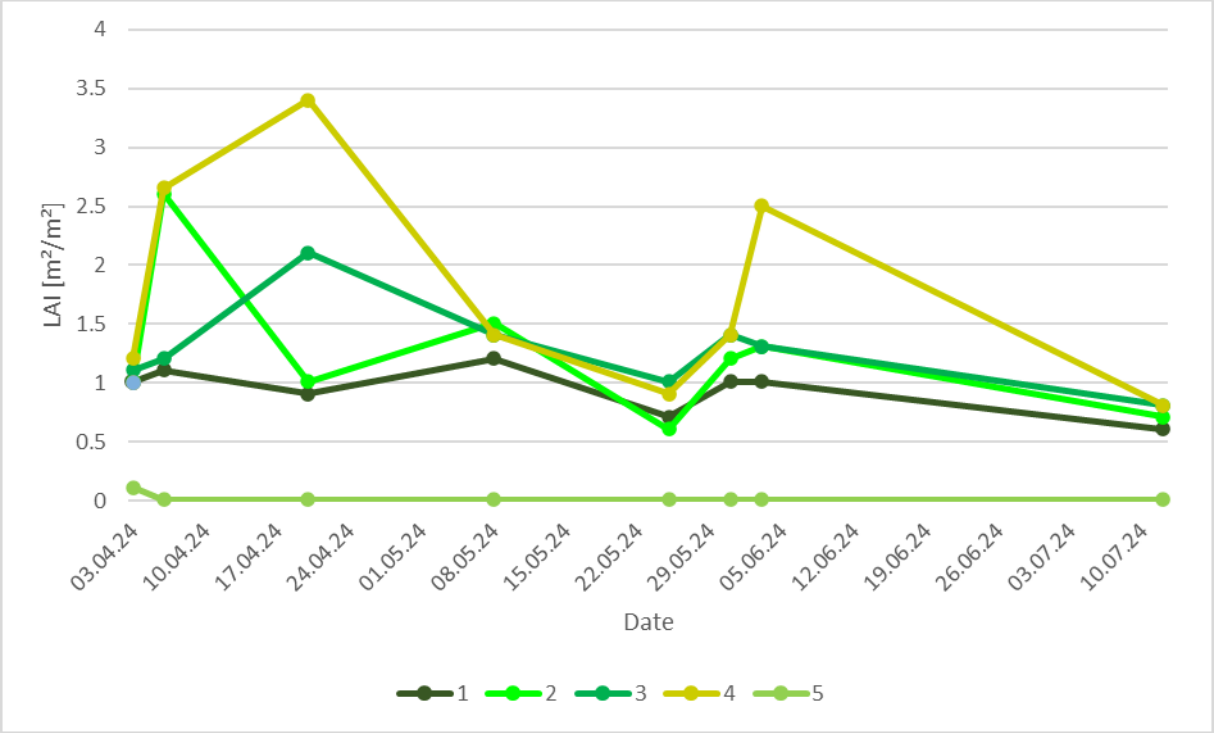

Figure 18 Leaf Area Index values calculated from PRISMA and EnMap data. Timeline at selected pixels at the Mali test-site. Numbers correspond with locations indicated in Figure 17.

4.3.1 Validation of Canopy and Leaf Water Content

Canopy Water Content was calculated using the Plant Water Retrieval (PWR) Tool available within the EnMap toolbox (Figure 19).

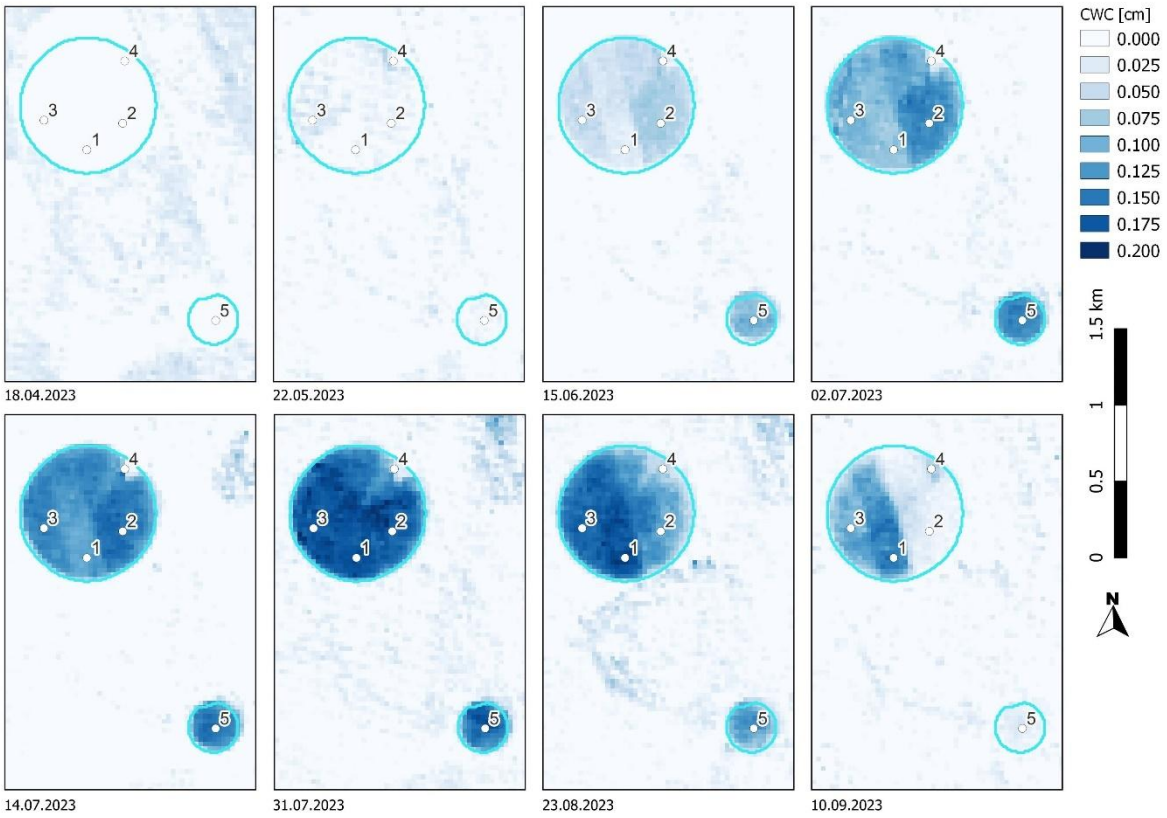

Figure 19 Canopy Water Content results calculated from PRISMA data acquired during the 2023 dry season at AKTC Zambia.

The method described in more detail in D07_ATBD_PS_I was developed by Wocher et al. 2018. Included in its implementation within the EnMap toolbox is a calibration factor which has been validated through performance assessment. The PWR tool has proven its ability to accurately predict plant water conditions as found in samples taken at winter wheat and corn test sites in Bavaria. The transferability of the method was also shown (Wocher et al. 2018). While validation with in-situ data still helps to prove the robustness of results, it is not strictly necessary. The method was chosen with regards to the unavailability of quantitative plant water data at the AKTC test site.

Leaf Water Content was then derived by combining LAI and CWC results (Figure 20 Leaf Water Content calculated from CWC and LAI derived from PRISMA data (31.07.2023)). As the intermediate products have already been validated or do not need validation, no separate validation has been conducted for LWC.

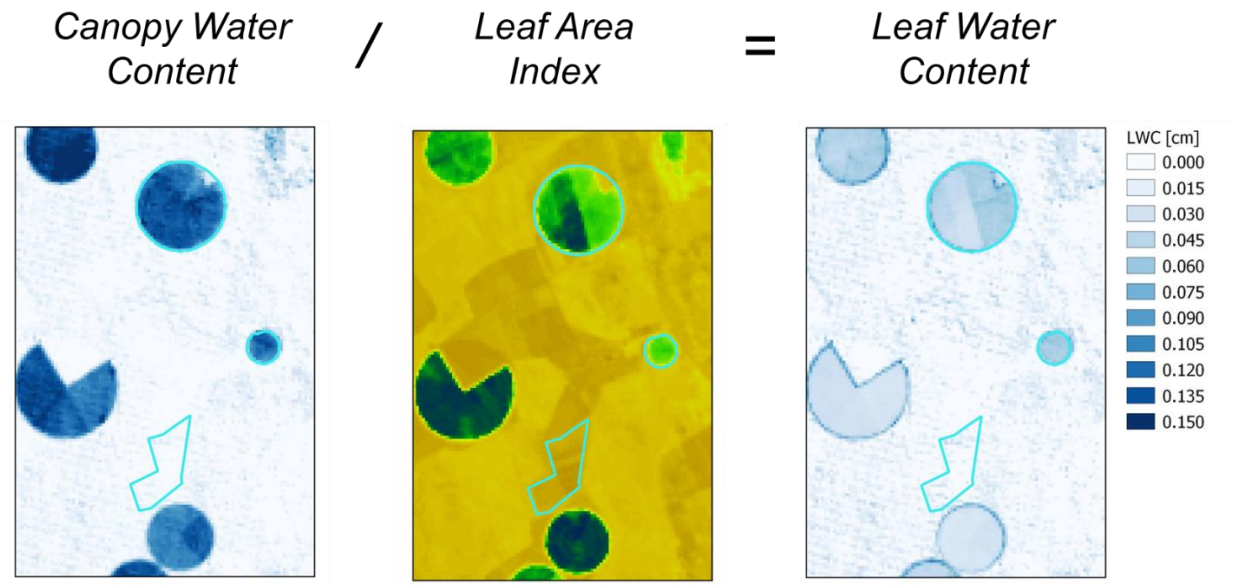

Figure 20 Leaf Water Content calculated from CWC and LAI derived from PRISMA data (31.07.2023)

While no validation as such is planned in the Mali test-site for the hyperspectral products, the time-series was also calculated there and is shown in the following figure.

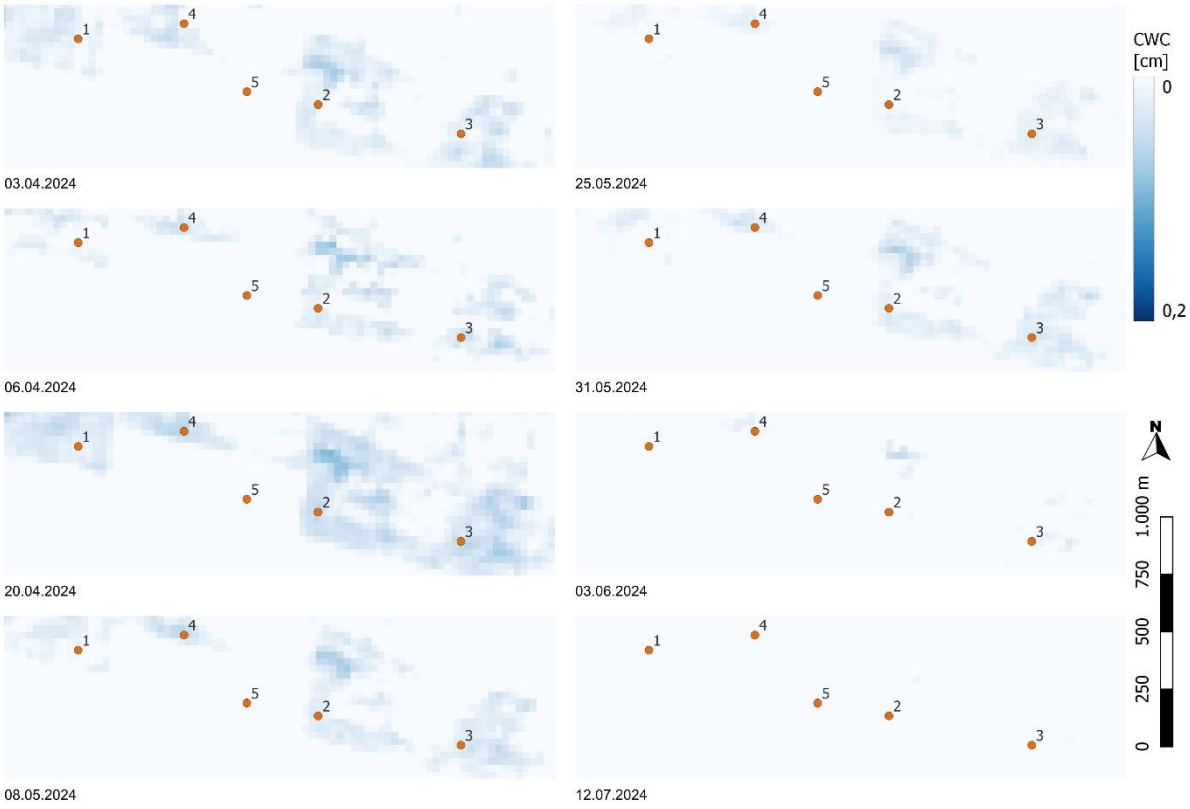

Figure 21 Canopy Water Content results calculated from PRISMA and EnMap data acquired in 2024 at the Mali test-site

5 Conclusion

One of the main challenges for the validation of the project results was the relatively sparse availability especially of quantitative in-situ validation data. We have thus in some cases resorted to external validation data (e.g. Soil Moisture Data from the International Soil Moisture Network, LAI data calculated from Sentinel-2 multispectral data). In other cases, our methods were chosen to include approaches that have been validated before (e.g. thermal sharpening and plant water retrieval).

List performed a sensitivity analysis of agricultural drought indices at 8-day and monthly scales, encompassing remote sensing indices such as ECOSTRESS ESI, SMAP SM, ESA SWI, STR, SDCI, and meteorological KBDI. In-situ measurements from the International Soil Moisture Network (ISMN) were employed as a reference to

understand the sensitivity of these indices to soil moisture variability. Results reveal SMAP's greater performance, followed by SWI. STR correlates with SM but includes scattered values. ECOSTRESS ESI effectively captures the spatial nuances of local drought stress; however, it is limited by temporal sampling frequency, impeding the variability analysis at intra-monthly scales. No single index universally excels, underscoring the need for further refinement. Advocating for a high-resolution RS data-driven drought index, this study provides insights for future mission applications (e.g., TRISHNA, SBG, LSTM), offering a roadmap for enhanced drought monitoring in Africa.

The products develop by Vito (Crop Water Stress Indicator) and Vista (LAI and CWC/LWC) would benefit from an improved availability of in-situ validation data, but in an expert interview with AKTC, the differences in development of the crops could be explained by the user.

6 References

Gao, F., Kustas, W. P., & Anderson, M. C. (2012). A Data Mining Approach for Sharpening Thermal Satellite Imagery over Land. *Remote Sensing 2012, Vol. 4, Pages 3287-3319*, *4*(11), 3287–3319. https://doi.org/10.3390/RS4113287

Guzinski, R., & Nieto, H. (2019). Evaluating the feasibility of using Sentinel-2 and Sentinel-3 satellites for high-resolution evapotranspiration estimations. *Remote Sensing of Environment*, *221*, 157–172. https://doi.org/10.1016/J.RSE.2018.11.019

Sanchez, J. M., Galve, J. M., Nieto, H., & Guzinski, R. (2024). Assessment of High-Resolution LST Derived from the Synergy of Sentinel-2 and Sentinel-3 in Agricultural Areas. *IEEE Journal of Selected Topics in Applied Earth Observations and Remote Sensing*, *17*, 916–928. https://doi.org/10.1109/JSTARS.2023.3335896

Verhoef, W., & Bach, H. (2007). Coupled soil-leaf-canopy and atmosphere radiative transfer modeling to simulate hyperspectral multi-angular surface reflectance and TOA radiance data. Remote Sensing of Environment, 109, 166−182. https://doi.org/10.1016/j.rse.2006.12.013

Wocher, M., Berger, K., Danner, M., Mauser, W., & Hank, T. (2018). Physically-Based Retrieval of Canopy Equivalent Water Thickness Using Hyperspectral Data. Remote Sensing, 10, 1924. https://doi.org/10.3390/rs10121924